Polymer 51 (2010) 5448–5455

Contents lists available at ScienceDirect

Polymer

journal homepage: www.elsevier.com/locate/polymer

Synthesis, characterization and degradation of biodegradable thermoplastic elastomers from poly(ester urethane)s and renewable soy protein isolate biopolymer

Wenshou Wang [a], Yanlin Guo [b], Joshua U. Otaigbe [a,*]

[a] School of Polymers & High Performance Materials, The University of Southern Mississippi, Hattiesburg, MS 39406-0076, United States
[b] Department of Biological Sciences, The University of Southern Mississippi, Hattiesburg, MS 39406-0076, United States

ARTICLE INFO

Article history:
Received 30 July 2010
Received in revised form
15 September 2010
Accepted 18 September 2010
Available online 27 September 2010

Keywords:
Poly(ester urethane)s
Soy protein isolates
Biodegradable polymers
Thermoplastic elastomers

ABSTRACT

New biodegradable poly(ester urethane)/soy protein isolate (PEU/SPI) hybrids were prepared by *in situ* polymerization. The chemical incorporation of the SPI into the backbone chain of the PEU was facilitated by the reaction of the amine functional groups of SPI with methylene diphenyl diisocyanate (MDI). X-ray diffraction results showed that the chemical incorporation of SPI into PEU significantly changed the molecular structure of the PEU. The PEU/SPI hybrids exhibited higher thermal decomposition temperature and significant increase in the modulus compared with that of pure PEU. Microscopic examination of the morphology of PEU/SPI hybrids confirmed very fine and homogeneous SPI dispersion in PEU. The hydrolytic degradation of the PEU in a phosphate buffer solution was accelerated by incorporation of SPI, which was confirmed by water absorption and scanning electron microscopy of the samples after up to 10 weeks immersion in the buffer solution. This study provides a facile and innovative method of controlling the biodegradation rate of pure PEU with the additional advantage of environmentally-benign biodegradation of the hybrid PEU/SPI polymer, making the concept potentially widely applicable.
Published by Elsevier Ltd.

1. Introduction

The development of synthetic petroleum-based polymer materials (such as polyethylene and polypropylene) has resulted in a number of serious environmental problems that is exacerbated by the fact that several metric tons of consumer plastics waste are designed to be discarded after use and need to be safely disposed [1]. A number of plastics waste disposal methods such as combustion and landfill are known to cause environmental pollution. For example, combustion of plastics waste can generate toxic air pollution and landfill can lead to underground water pollution and soil contamination. In this context, biodegradable polymers could help solve the above problems because they can be made to degrade in an environmentally-benign way by the action of humidity and microorganisms. Consequently, research efforts towards developing environmentally-friendly and biodegradable polymers and their hybrids with other compatible materials for various applications have gained significant attention in recent years in academia and industry.

Examples of biodegradable polymers include polyester, polycarbonate, protein, starch, and cellulose [2–5]. In the class of polymers just mentioned, polyurethane is a very important industrial material because of its special properties and relatively mature production equipment and technology in industry [6–9]. It is well known that the glass transition temperature and mechanical properties of polyurethanes can be tuned by changing the composition and ratio of the soft and hard segments to yield a wide range of polyurethanes that varies from thermoplastic elastomers to rigid thermoset foams. Poly(ε-caprolactone)-based polyurethane is one example of a widely studied biodegradable elastomer because of its good mechanical properties and biocompatibility that are highly desirable in a number of uses such as cardiovascular stents and scaffolds in biomedical engineering [10–12]. One major drawback of the poly(ε-caprolactone) (PCL)-based polyurethane in the applications just mentioned is that it degrades very slowly (i.e., it may take years to degrade completely) in natural environments because of its intrinsic hydrophobic nature. Another limitation of the PCL-based polyurethane is its relative high cost compared with that of natural renewable biodegradable polymers such as

* Corresponding author. Tel.: +1 601 266 5596.
E-mail address: Joshua.Otaigbe@usm.edu (J.U. Otaigbe).

0032-3861/$ – see front matter Published by Elsevier Ltd.
doi:10.1016/j.polymer.2010.09.056

cellulose, starch, soy protein, and chitin that are derived from agricultural biopolymers [13–16].

In the class of biodegradable polymers already mentioned, soy protein isolate has been studied extensively as an alternative material to petroleum-based polymers due to its relative low cost, availability, and biodegradability [17–22]. Soy protein isolate (SPI) is prepared from soybean seeds that contain at least 90% proteins with molecular weights ranging from 8 kDa to about 600 kDa. The various components of SPI are identified as 2S, 7S, 11S, and 15S (S denotes Svedberg unit), and are respectively found in 20–27%, 37%, 31–40%, and 10–11% of the total weight in the SPI [23]. The 7S or β-conglycinin (42–58 kDa) and 11S or glycinin (360 kDa) are reported to be the two major globulins present in SPI. These proteins can react with each other to form various crosslinkages such as disulphide, lysinoalanine, and lanthionine. The resin obtained from SPI is very brittle and hence difficult to process and use. Another inherent characteristic of SPI is its strong tendency to absorb moisture, leading to its relatively fast degradation in moist environments [24]. A number of researchers have reported attempts to improve the processability of SPI plastics by using relatively high concentrations of plasticizers (e.g., water, glycerol and waterborne polyurethane) in the SPI plastic batch formulation [25–28].

In previous articles, we reported innovative synthesis and processing of useful biodegradable and bioabsorbable polymers such as poly(ester urethane)s [10,12] and soy protein isolates [18,29,30] with improved properties. The work described in this current article aims to extend our prior research into feasibility of developing new poly(ester urethane)/soy protein hybrids that combines in one material the advantages of polyurethanes (excellent mechanical properties and biocompatibility) and SPI (low cost, environmentally-benign degradation in humid environments, and availability from renewable natural resources). In this paper, we specifically report an innovative method of chemically incorporating SPI into the backbone chain structure of poly(ester urethane) via *in situ* polymerization. The resulting thermomechanical properties, degradation behavior, and interaction between the poly (ester urethane) and SPI in the hybrids are studied to assess the benefits of the new PEU/SPI hybrid materials. It is hoped that the current results reported in this article may stimulate a better understanding of the behavior of the materials in a number of applications requiring the biocompatibility and bioabsorbability of the hybrid components.

2. Experimental section

2.1. Materials

Poly(ε-caprolactone) diol (TONE® Polyol 5249; Mn = 2000) was purchased from Dow Chemical Company (Midland, MI). Methylene diphenyl diisocyanate, toluene, dibutyltin dilaurate, 1,4-butanediol and phosphate buffer solution (1 M, pH = 7.4) were obtained from Sigma Aldrich. Soy protein isolate was purchased from the Solae Company (St. Louis, MO).

2.2. Synthesis of polyurethane/soy protein isolate (SPI) hybrids

The desired amount of the soy protein isolate was dispersed in toluene in a dry reaction flask. The flask was subsequently placed in an ultrasonic bath for 2 h in order to homogeneously disperse the SPI in toluene. Subsequently, PCL diol was added to the flask and the flask was placed in an isothermal oil bath (65 °C) under stirring. After the PCL diol was dissolved completely, dibutyltin dilaurate and methylene diphenyl diisocyanate were added to the reaction system. After 3 h, 1,4-butanediol was added to the system and the reaction was allowed to continue for another 3 h to yield the final product. The feed ratios of the reactants and starting materials are summarized in Table 1. All the as-polymerized samples were dried under vacuum oven for 24 h and compression molded at 150 °C into the film configurations used for the following measurements.

Table 1
The feed ratio of the synthesized PEU/SPI hybrids.

Code	PCL diol (g)	MDI (g)	1,4-Butanediol (g)	Soy Protein Isolate (g)
PEU	5	2.21	0.5	0
PEU/3% SPI	5	2.21	0.5	0.23
PEU/6% SPI	5	2.21	0.5	0.46
PEU/10% SPI	5	2.21	0.5	0.77
PEU/20% SPI	5	2.21	0.5	1.54

2.3. Measurements

2.3.1. FT-IR and XRD

IR spectroscopy was conducted on the samples using a Nicolet 6700 FT-IR spectrometer (Thermo Fisher Scientific, NH). The crystallinity of the PEU/SPI hybrids was evaluated using X-ray diffraction (XRD) analysis. A Rigaku Ultima III powder diffractometer was used, employing Cu Kα radiation (at 40 kV and 44 mA). The XRD data were collected over the range of $2\theta = 3–40^\circ$ at a rate of 1°/min.

2.3.2. Thermal analysis

Differential scanning calorimetry (DSC) was carried out on the samples over a temperature range of −80 °C to 250 °C using a TA Instruments (TA Q100) operating under a nitrogen atmosphere. The DSC heating or cooling rate was 10 °C/min. The midpoint of the transition zone was taken as the glass transition temperature (T_g) of the sample. Thermogravimetric analysis (TGA) tests were conducted on the samples using Perkin–Elmer (Pyris 1 TGA) equipment operating over a temperature range of 50–800 °C and a heating rate of 10 °C/min under a nitrogen atmosphere. Thermal decomposition temperature was defined as the temperature corresponding to the maximum rate of weight loss.

2.3.3. Static and dynamic mechanical properties

Static mechanical tensile stress–strain measurements were performed on the samples using a Material Testing System Alliance RT/10 and a MTS Testworks 4 computer software package for automatic control of test sequences and data acquisition and analysis. Dumbbell-shaped test specimens (with an effective cross section of 4 × 0.7 mm^2) were cut from the compression molded PEU/SPI films and tested at room temperature and using a crosshead speed of 20 mm/min according to the ASTM D882-88 standard method. The tests were performed in triplicate to give the mean values reported in this paper. The temperature dependencies of the dynamic storage modulus E′ and mechanical damping ($\tan\delta$) of the compression molded rectangular test specimens (20 × 5 × 1 mm^3) were determined using a PYRIS Diamond Dynamic Mechanical Analyzer (DMA) operating at temperatures ranging from −80 °C to 150 °C, a heating rate of 3 °C/min, a frequency of 1 Hz, and a linear strain amplitude of 10%.

2.3.4. Hydrolytic degradation in buffer solution

The degradation test was conducted in a phosphate buffer solution of pH = 7.4 at 37 °C following procedures reported elsewhere [31]. The samples were cut into disks (diameter = 15 mm and thickness = 1 mm) and placed into the buffer solution (pH = 7.4) at 37 °C. The original weight of the sample was recorded as W_0. When the sample was taken out of the buffer solution and

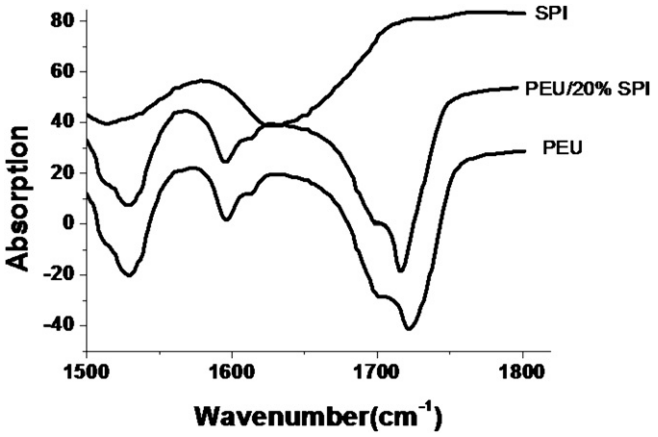

Fig. 1. Typical IR spectra of pure PEU and PEU/SPI hybrids.

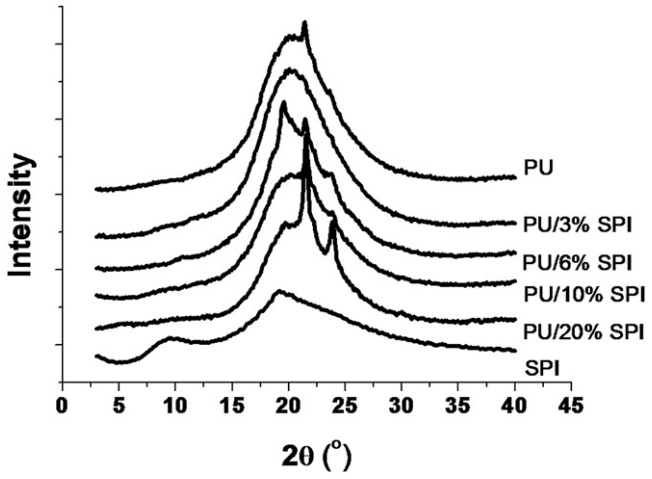

Fig. 2. XRD data of pure PEU and PEU/SPI hybrids.

the excess water of the surface was removed with a tissue paper, its weight was recorded as W_1. The sample weight after drying in a vacuum oven at 30 °C for at least 48 h was recorded as W_2. The percent water absorbed (W_{ab}) was calculated from $100 \times (W_1 - W_2)/W_2$; and the weight loss ($W_{loss}$) was calculated from $100 \times (W_0 - W_2)/W_0$.

2.3.5. Thin film formation and microscopic analysis

The as-synthesized PEU/SPI polymer containing the desired concentration of SPI was dissolved in dimethylformamide (DMF) to yield a 2% solution of the polymer. Subsequently, a portion of this solution was carefully dropped onto a coverslip (12 mm diameter) to form a thin film. The coverslips were left at room temperature for 48 h, and then were further dried under vacuum for additional 48 h.

The structure of the PEU/SPI thin films was examined with an Olympus microscope (BX60) under a phase contrast lens or a fluorescence lens with the filter set for the examination of FITC (fluorescein isothiocyanate). The images were photographed with a micropublisher digital camera (Qimaging) and processed using Image-Pro Plus software. The PEU/SPI thin films were further analyzed with a Zeiss LSM 510 laser-scanning confocal microscope under the configuration of excitation at 488 nm and emission at 505 nm. The 3D projection was reconstructed from Z-stack sections with LSM Image Examiner software (Zeiss). For scanning electron microscopy (SEM) analysis, the surfaces of the thin films were sputter-coated with gold at 25 mA for 150 s to increase the electrical conductivity and then analyzed with a SEM (FEI Quanta 200) under high vacuum at 20 kV.

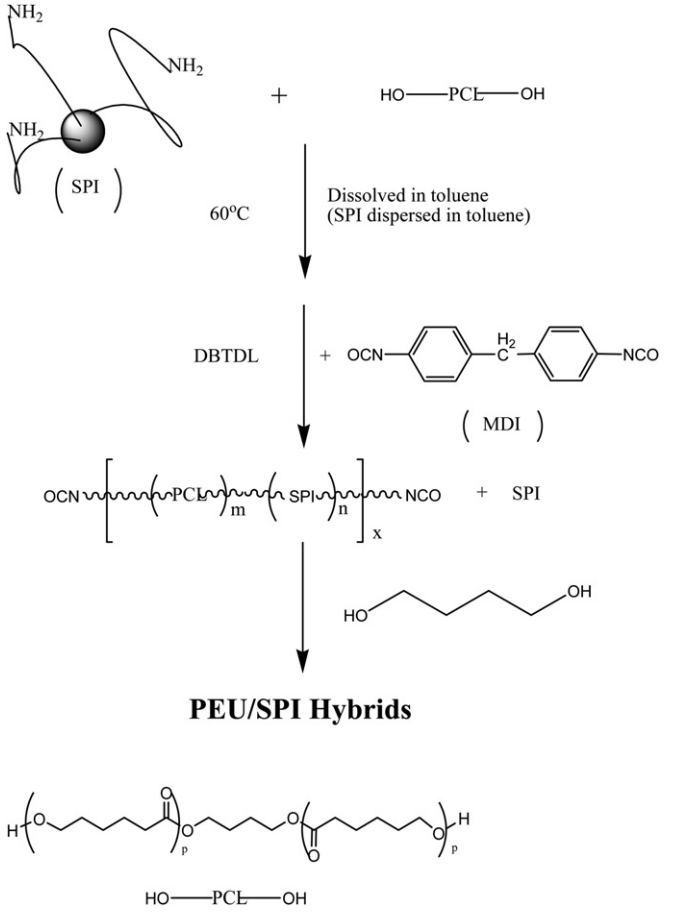

Scheme 1. The synthesis route of PEU/SPI hybrids.

3. Results and discussion

3.1. The synthesis and chemical structure of PEU/SPI hybrids

In order to study the effects of SPI content on the properties of PEU/SPI hybrids, a series of PEU/SPI hybrids with different SPI contents were synthesized as already described. Fig. 1 shows the IR spectra of the PEU/SPI hybrid system. Clearly, the pure SPI

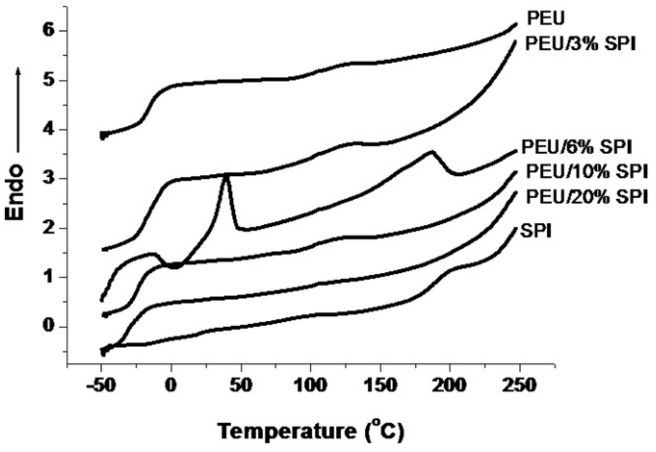

Fig. 3. DSC data of pure PEU and PEU/SPI hybrids.

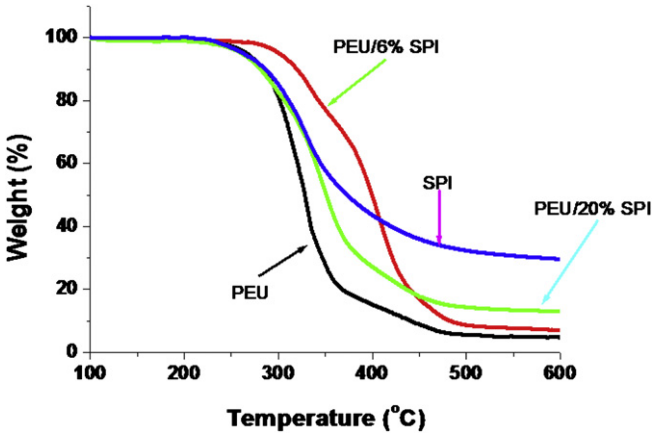

Fig. 4. TGA data of pure PEU and PEU/SPI hybrids.

exhibits two absorptions at 1535 and 1625 cm^{-1} that are attributed to carbonyl and amide groups of SPI [32]. The two absorption peaks occurring at 1702 cm^{-1} and 1723 cm^{-1} are ascribed to the vibration of carbonyl groups of the polyurethane. The absorption of PEU at 1723 cm^{-1} is shifted to a lower wavenumber (i.e., 1715 cm^{-1}), indicating strong hydrogen bonding between PEU and SPI in the hybrid system (Scheme 1).

The crystallinity of the PEU/SPI hybrids was studied by XRD analysis and the data obtained are summarized in Fig. 2. A relatively sharp peak at $2\theta = 21.4^\circ$ and a broad shoulder peak are clearly evident for the pure PEU in this figure. In contrast, the pure SPI revealed two broad peaks around $2\theta = 9.6^\circ$ and 19.2°. Clearly, the incorporation of SPI into PEU in the hybrid system has a discernable effect on the crystallinity of PEU as Fig. 2 shows. It is worthy to note that no sharp peak was observed for the PEU/3% SPI hybrid while two sharp peaks at $2\theta = 19.5^\circ$ and 21.4° were observed for the PEU/6% SPI and only one peak was observed at $2\theta = 21.4^\circ$ for the PEU/10% SPI hybrid. In addition, two peaks at $2\theta = 21.4^\circ$ and 24° are clearly evident for the PEU/20% SPI. These XRD results imply that the PEU/SPI hybrids with different SPI concentrations have different crystalline and microcrystalline structures that are thought to be a consequence of the strong physicochemical interactions between the SPI and PEU in the hybrid system. For example, there will be hydrogen bonding between the carbonyl and amide groups of SPI and PEU, and a portion of the amine groups of the SPI will react with MDI thereby facilitating incorporation of the SPI into the backbone chain of PEU via covalent linkages. This is an important and facile strategy for introducing renewable, biodegradable components such as SPI into already existing polymer systems such as polyurethanes.

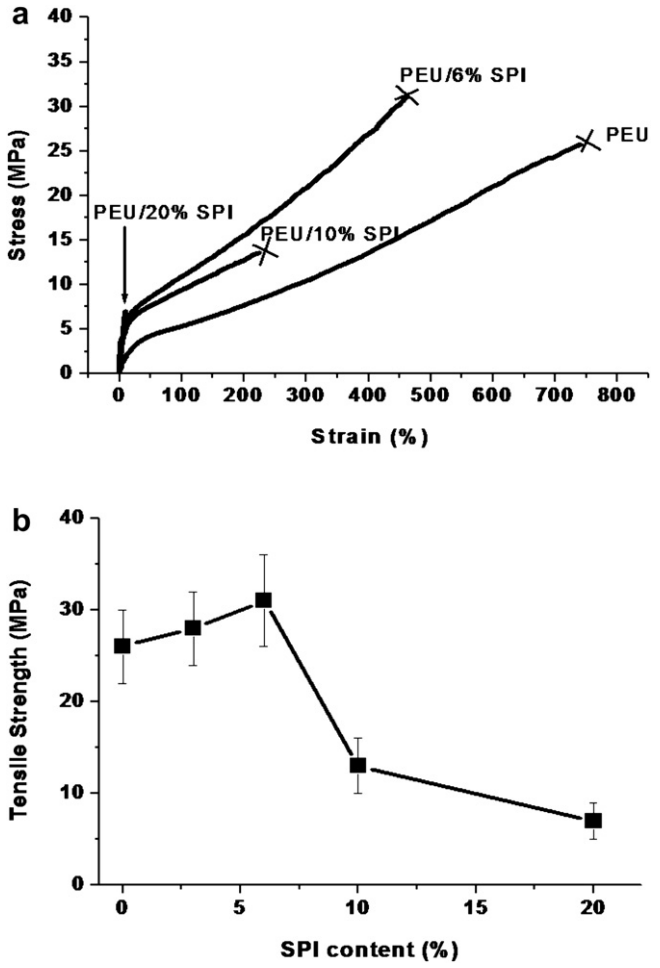

Fig. 5. Typical stress–strain curves (a) and tensile strength dependence on SPI content (b) of PEU and PEU/SPI hybrids. Note that data for the PEU/3% SPI hybrid is not shown in (a) for the purpose of clarity and to avoid cluttering of data.

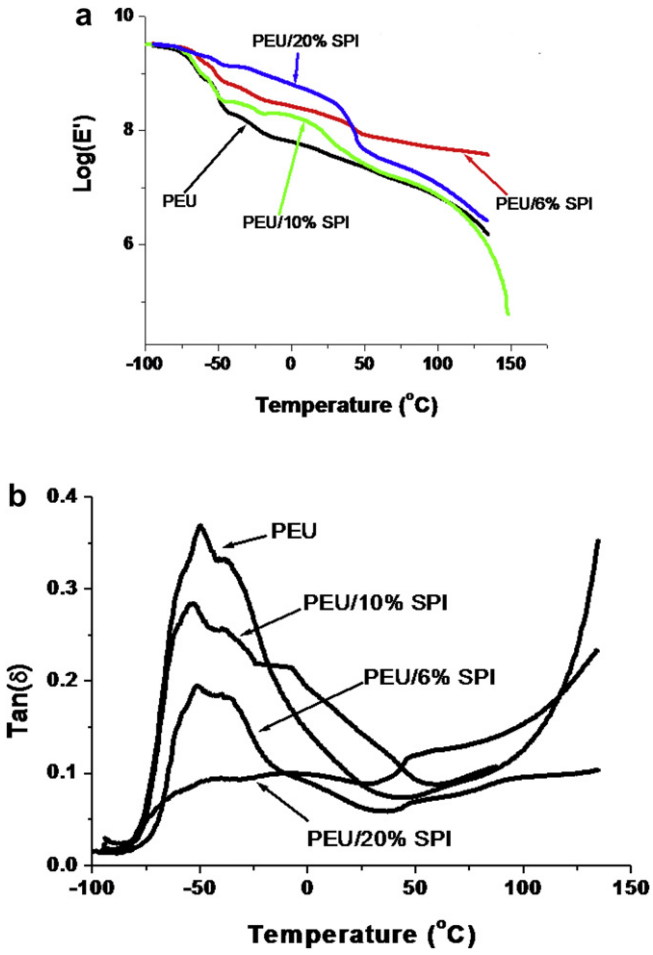

Fig. 6. Temperature dependencies of storage modulus (a) and tanδ (b) of pure PEU and PEU/SPI hybrids. Note that data for the PEU/3% SPI hybrid is not shown for the purpose of clarity and to avoid cluttering of data.

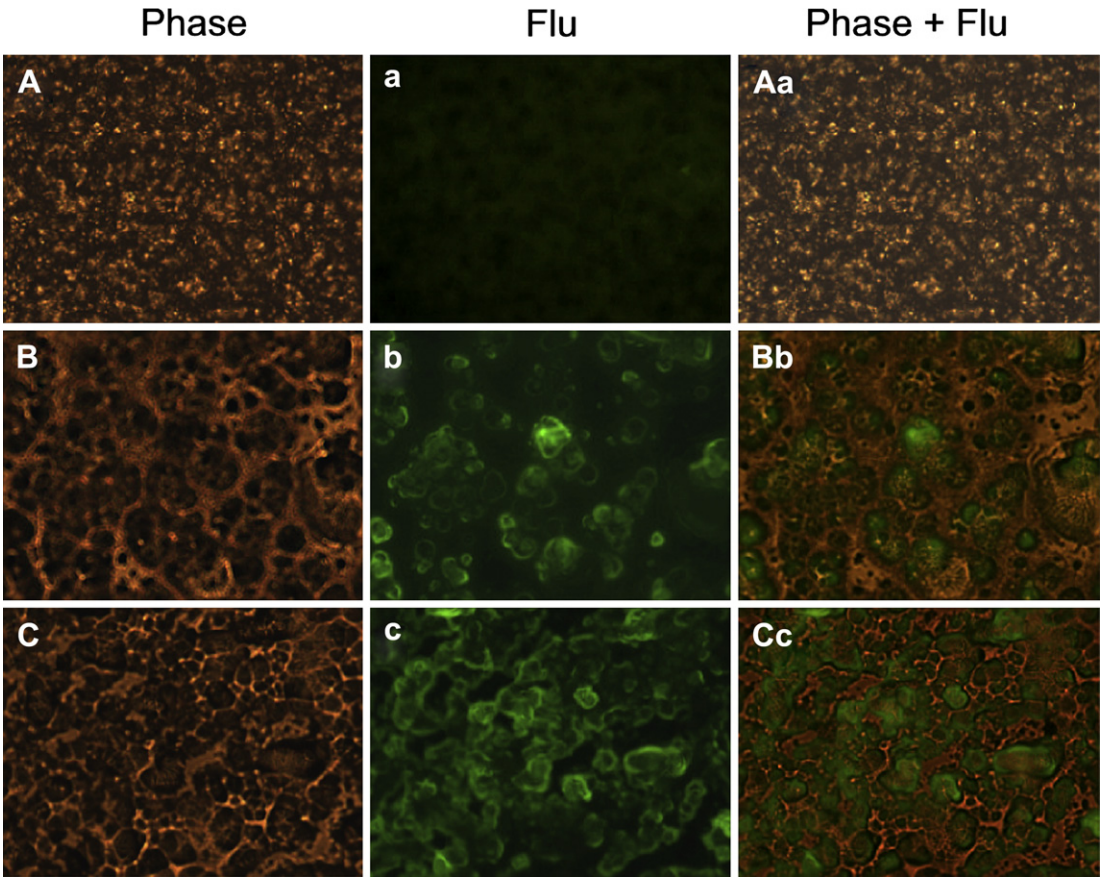

Fig. 7. Microscopic analysis of architecture and surface topology of thin films made from pure PEU film (A, a, Aa), PEU/10% SPI (B, b, Bb), and PEU/20% SPI (C, c, Cc). The images were acquired with an Olympus microscope (magnification = 1000×) under a phase contrast lens (A–C), fluorescence lens (a–c, with filters set for FITC) or fluorescence lens under simultaneous illumination of regular light (Aa–Cc).

3.2. Thermal analysis

The thermal properties of the PEU/SPI hybrids were studied by DSC and TGA as already described. The results obtained are depicted in Fig. 3 showing thermograms obtained from the samples after second heating runs. For the pure PEU, two glass transition temperatures were observed at −14 °C and 110 °C, corresponding to the glass transition temperatures of the PEU soft and hard segments, respectively. For the PEU/3% SPI hybrid, the glass transition temperature of the soft segment is relatively unaffected while the glass transition temperature region of the hard segment is broadened and shifted to a lower temperature (i.e., 105 °C). The peak at 40 °C observed for the PEU/6% SPI corresponds to the melting point of the soft segment (i.e., PCL) of the PEU of this study while the exothermic transition at 187 °C is attributed to the protein aggregation of the SPI in the hybrid system [17,33]. At SPI concentration of 10% in the PEU/SPI hybrid, the melting peaks for both soft and hard segments disappeared and the glass transition temperatures of the soft and hard segments were respectively shifted to −23 °C and 106 °C. For the PEU/20% SPI hybrid, the glass transition temperature of the soft segment is shifted to −29 °C while the hard segment glass transition temperature is not evident

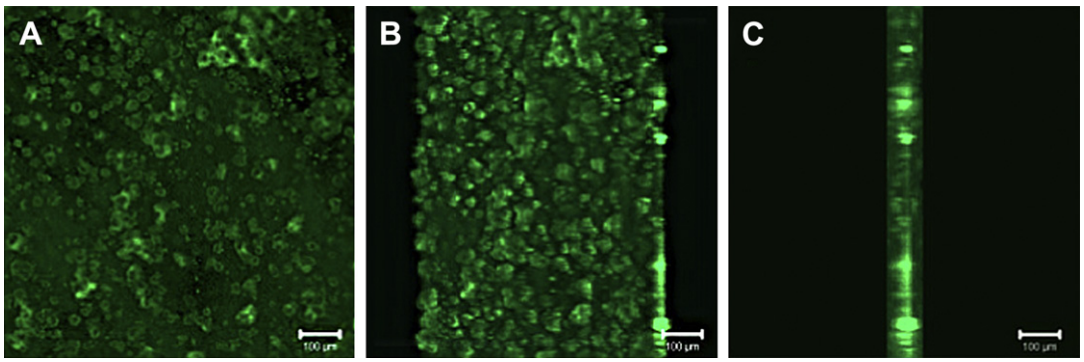

Fig. 8. Laser scanning microscopic analysis of PEU/10% SPI thin film. The film was examined under the configuration of excitation at 488 nm and emission at 505 nm. The 3D projection of the surface structure was reconstructed from a Z-stack consisting of 64 sections (1.5 μm/section). The image was viewed from three different directions: A, front view; B, front view with an angle; C, cross section.

in Fig. 3. For the pure SPI, only an exothermic transition is observed, which is attributed to the protein aggregation of the SPI [17]. Clearly, the preceding results show that the thermal properties of the PEU/SPI hybrids are influenced by the SPI content and the nature of both the soft and hard segments of the PEU. Because of the chemical incorporation of the SPI into the PEU macromolecular backbone via crosslinking by MDI already mentioned, the effects of hydrogen bonding between the soft and hard segments of the PEU, as well as, between the SPI and PEU segments are such that the glass transition temperature decreases in a manner that is consistent with the hypothesis of nanostructuration via (covalent) crosslinking by diisocyanates already mentioned.

The thermal stability of the PEU/SPI hybrids was evaluated via TGA and the results obtained are shown in Fig. 4. The decomposition temperatures for the pure PEU and pure SPI are 319 °C and 336 °C, respectively. The decomposition temperature of PEU increased with the incorporation of SPI. The PEU/6% SPI hybrid was found to exhibit the highest decomposition temperature. The observed behavior of the PEU/6% SPI hybrid is remarkably different from that of the other hybrid compositions studied. Two crystallinity peaks and two melting peaks were respectively observed in XRD and DSC for the hybrid composition just mentioned. The highest decomposition temperature observed is thought to be due to the observed crystalline structure of the hybrids that is facilitated by the strong chemical compatibility of the PEU and SPI as already mentioned.

3.3. Static and dynamic mechanical properties

Typical stress–strain and tensile strength data of PEU/SPI hybrids are shown in Fig. 5. Clearly, the elongation at break is significantly decreased by the incorporation of SPI into the hybrid system (Fig. 5a). The tensile strength data of the hybrids (Fig. 5b) shows an interesting trend. At low concentrations of the SPI in the hybrid (i.e., <6% SPI) the tensile strength increases with increasing SPI content. This behavior is followed by a relatively sharp decrease in tensile strength with increasing SPI content at the high SPI concentrations (i.e., >6% SPI). One plausible interpretation of these findings is that at low SPI content (3%–6%), the SPI is mostly incorporated into the backbone chain of the PEU thereby acting as a reinforcing filler at the molecular level (or nanofiller) in both soft and hard segments of the PEU with significantly enhanced interactions between the SPI and PEU in the hybrid system, increasing the observed tensile strength. At relatively higher SPI concentrations a portion of the SPI will phase segregate thereby leading to lower tensile strength caused by the relatively poor interface between the PEU and SPI components of the hybrid.

The temperature dependence of the storage modulus of the PEU/SPI hybrids was measured by DMA and the results obtained are shown in Fig. 6. Obviously, the modulus of PEU significantly increased by incorporation of the SPI, especially in the temperature range of −50 °C to 50 °C corresponding respectively to the glass transition and melt temperatures of the soft segment of the PEU (Fig. 6a). This finding is consistent with the fact that the glass transition temperature of SPI [20] is higher than the melt temperature of the soft segment of PEU. Therefore, in the temperature range just mentioned the SPI is in the glassy state and should lead to an increase in the modulus of the PEU/SPI hybrids compared to that of the pure PEU. The glass transition temperature of PEU/SPI hybrids measured by DMA is shown in Fig. 6b. Like the DSC data already discussed, the glass transition temperature of PEU in the hybrid is decreased by the SPI incorporation with the PEU/20% SPI hybrid composition showing a relatively anomalous behavior that is characterized by a broad relaxation process occurring at the T_g, making it difficult to extract the T_g from the data depicted in Fig. 6b.

3.4. The Surface structure and morphology of PEU/SPI hybrids

When examined under a phase contrast microscope, the surface of the pure PEU film was covered with polymer particles with fairly uniform distribution (Fig. 7A). Incorporation of SPI into the PEU significantly altered the surface structure (Fig. 7B and C). An interesting fortuitous finding is that the structural features of PEU/SPI thin films were better revealed under a fluorescence microscope due to the auto-fluorescence of SPI. As shown in Fig. 7a, the film formed from pure PEU emits a dim green fluorescence while the SPI was detected as bright green particles (Fig. 7b and c). When the samples were illuminated simultaneously with regular and fluorescence light, the PEU was detected as a matrix-like structure (Fig. 7Bb and Cc, brown) where the SPI portion was seen as green particles nicely embedded in the matrix (Fig. 7Bb and Cc, green).

We further analyzed the structure of PEU/10% SPI hybrid film by using a confocal laser-scanning microscope to view the surface structure of the thin film from different directions as well as its internal cross section. Fig. 8 shows a three-dimensional projection of the thin film reconstructed form a Z-stack consisting of a series of sections and viewed from three different directions. Clearly, these images demonstrate the close interaction and integration between PEU matrix (Fig. 8, dark green background) and SPI particles (Fig. 8, bright green). Fig. 8A shows a direct front view of the thin film surface; Fig. 8B is an image of the surface viewed from an angle of approximately 30°, while Fig. 8C represents the cross section of the thin film showing the thickness. Similar to the images obtained

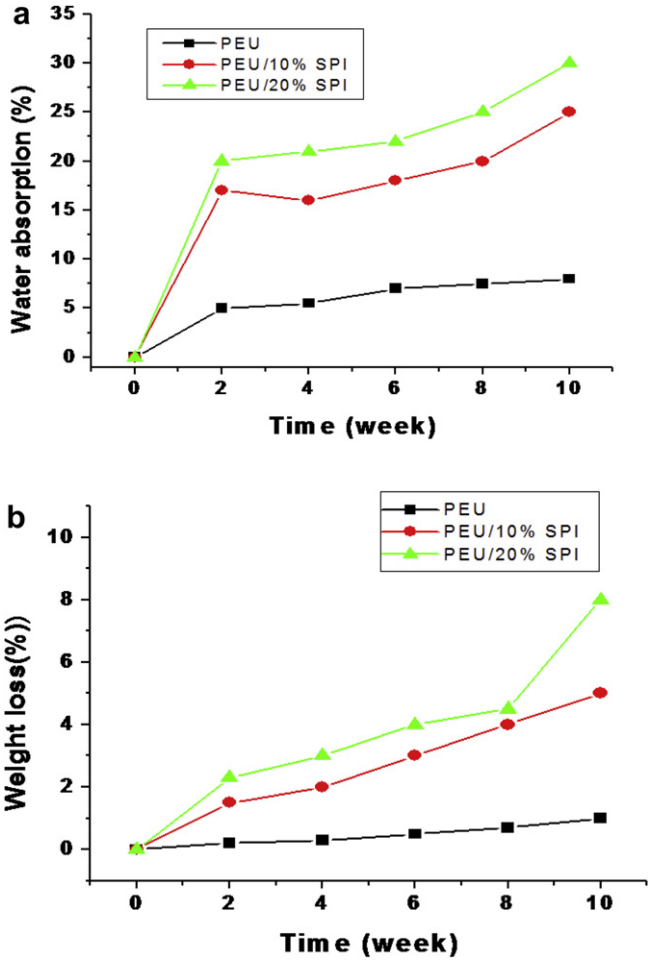

Fig. 9. Water absorption (a) and weight loss (b) of pure PEU and PEU/SPI hybrids.

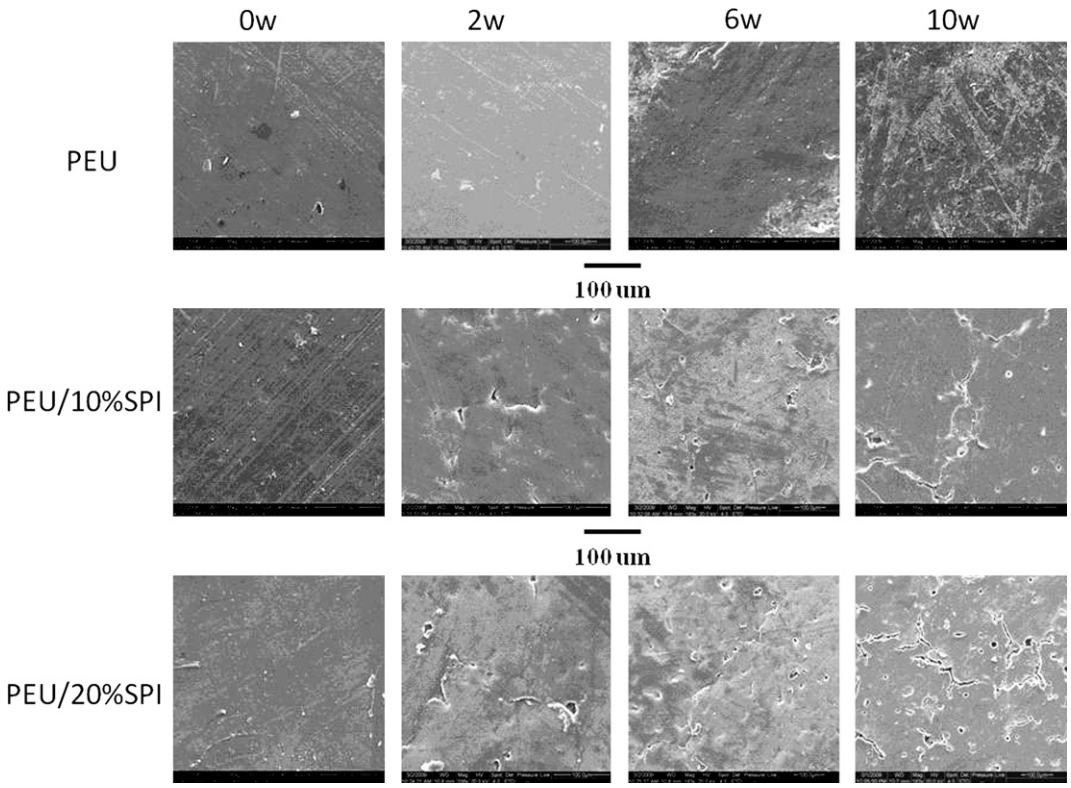

Fig. 10. The surface morphology of pure PEU and PEU/SPI hybrids after different weeks (0–10 w) of hydrolytic degradation as described in the text.

with conventional fluorescence microscopy (Fig. 7b and c), the dark green background represents PEU matrix with integrated fine particles of SPI (or soy proteins at single molecule level). Bright green SPI particles with various sizes (Fig. 8A and B) may represent the aggregates that could not be completely dispersed in the solvent. The particle size was also measured with a commercial image analysis software (Image J®). The data obtained from the analysis just mentioned illustrates a monomodal distribution of the SPI particles with average size of approximately 30 μm (data not shown), which is well within the range determined by microscopy. In spite of variation in size, the overall distribution of SPI particles is reasonably well distributed within the PEU matrix thereby indicating the good integration of the two components in the hybrid system.

3.5. Hydrolytic degradation behavior

It is generally accepted that water absorption is favorable to the hydrolytic degradation of polymers. Therefore, in a typical hydrolytic degradation test the rate of water absorption (or sample weight gain) can be correlated with sample weight loss.

Fig. 9a shows the water absorption of PEU/SPI hybrids over a period of 10 weeks. For the pure PEU, water absorption is approximately constant at 5 wt% over a period of ten weeks. The water absorption increases significantly with increasing SPI content for the PEU/SPI hybrids compared with that of the pure PEU. This is understandable because SPI is more likely to absorb water than PEU. Fig. 9b shows the weight loss of the PEU/SPI hybrids after ten weeks of immersion in the buffer solution. For pure PEU the observed weight change after ten weeks of immersion in the solution is about 1 wt%. This weight loss is probably caused by the dissolution of unreacted monomers and oligomers. It is well known that PEU based on PCL degrades in water slowly. The observed weight loss is respectively 5 wt% and 9 wt% for PEU/10% SPI and PEU/20% SPI hybrids after ten weeks of immersion in the buffer solution, implying that incorporation of SPI into PEU (as in the current study) accelerates the degradation rate of PEU. This is an important result that may provide a facile method of controlling the degradation rate of pure PEU with the additional advantage of environmentally-benign biodegradation of the polymers.

In order to better understand the role of SPI on the degradation behavior of PEU, the morphology of PEU/SPI hybrids after different stages of degradation was studied by SEM and the results obtained are shown in Fig. 10. Clearly, the figure shows that after two weeks of immersion no obvious surface change in the sample surface morphology was observed for pure PEU as compared with that of the PEU/SPI hybrids. The PEU/SPI hybrids revealed holes and cracks on the surfaces of PEU/10% SPI and PEU/20% SPI that are ascribed to the degradation of the SPI moiety. It is worthy to note that after 10 weeks of immersion in the buffer solution, the surface of pure PEU is relatively intact (no cracks or holes), showing some evidence of surface roughness which is attributed to swelling of the sample caused by absorbed water. On the other hand, the PEU/SPI hybrids after ten weeks of immersion showed large cracks and holes and the samples were observed to be very close to disintegration. This observation is due to the preferential dissolution of the well dispersed SPI moieties, exposing more surfaces of the PEU fraction to water thereby accelerating the PEU degradation.

4. Conclusion

New biodegradable poly(ester urethane)/soy protein isolate hybrids with excellent properties were successfully prepared by *in situ* polymerization. The thermal stability and storage modulus of poly(ester urethane) (PEU) were enhanced by incorporation of SPI. Microscopic examination of the hybrids via optical, fluorescence and confocal microscopy revealed that SPI was homogeneously dispersed in the continuous PEU phase with a SPI particle size of

approximately 30 μm. The hydrolytic degradation of PEU was accelerated by incorporation of the SPI, providing a facile and an environmentally-benign innovative method of controlling the degradation rate of PEU and other chemically compatible biodegradable polymers.

Acknowledgments

This work was funded by the Chemical, Bioengineering, Environmental, and Transport Systems division of the U.S. National Science Foundation through a contract grant CBET 0752150. We thank Baobin Kang for microscopy analysis and Mississippi Functional Genomics Network for the use of the facility.

References

[1] Business Communications Company. Plast Eng 1994;50:34–5.
[2] Lapitsky Y, Zahir T, Shoichet MS. Biomacromolecules 2008;9:166–74.
[3] Yang KK, Wang XL, Wang YZ. J Ind Eng Chem 2007;13:485–500.
[4] Jahno VD, Ribeiro GB, Santos LA, Ligabue R, Einloft S, Ferreira MR, et al. J Biomed Mater Res Part A 2007;83A:209–15.
[5] Sitharaman B, Shi XF, Tran LA, Spicer PP, Rusakova I, Wilson LJ, et al. J Biomater Sci Polym Ed 2007;18:655–71.
[6] Rockwood DN, Woodhouse KA, Fromstein JD, Chase DB, Rabolt JF. J Biomater Sci Polym Ed 2007;18:743–58.
[7] Helminen A, Kylma J, Tuominen J, Seppala JV. Polym Eng Sci 2000;40:1655–62.
[8] Guan JJ, Wagner WR. Biomacromolecules 2005;6:2833–42.
[9] Guan JJ, Fujimoto KL, Sacks MS, Wagner WR. Biomaterials 2005;26:3961–71.
[10] Wang W, Ping P, Yu H, Chen X, Jing X. J Polym Sci Part A Polym Chem 2006;46:5505–12.
[11] Atzet S, Curtin S, Trinh P, Bryant S, Ratner B. Biomacromolecules 2008;9:3370–7.
[12] Ping P, Wang WS, Chen XS, Jing XB. Biomacromolecules 2005;6:587–92.
[13] Otey FH, Westhoff RP, Doane WM. Ind Eng Chem Res 1987;26:1659.
[14] Cai H, Dave V, Gross RA, McCarthy SP. J Polym Sci 1996;34:2701.
[15] Maache-Rezzoug Z, Zarguili I, Loisel C, Queveau D, Buleon A. Carbohydr Polym 2008;74:802–12.
[16] Gardner DJ, Oporto GS, Mills R, Samir MASA. J Adhen Sci Technol 2008;22:545–67.
[17] Mo X, Sun XS, Wang Y. J Appl Polym Sci 1999;73:2595–602.
[18] Otaigbe J, Adams D. J Environ Polym Degrad 1994;2:211. See also Otaigbe JU, Goel H, Babcock T, Jane J. J. Elastomers and Plastics 1999;31:56–71.
[19] Paetau I, Chen C, Jane J. Ind Eng Chem Res 1821;1994:33.
[20] Mo X, Sun X. J Polym Environ 2000;8:161–6.
[21] Lodha P, Netravali AN. J Mater Sci 2002;37:3657–65.
[22] Sue HJ, Wang S, Jane JL. Polymer 1997;38:5035–40.
[23] Hermansson AM. J Texture Stud 1997;9:33–58.
[24] Otaigbe JU. Plast Eng; 1998, April:37–9.
[25] Zhang J, Mungara P, Jane J. Polymer 2001;42:2569–78.
[26] Wang N, Zhang L. Polym Int 2005;54:233–9.
[27] Wang N, Zhang L, Gu J. J Appl Polym Sci 2005;95:465–73.
[28] Wang S, Sue HJ, Jane J. J Macromol Sci Pure Appl Chem 1996;33:557.
[29] Kurose T, Urman K, Otaigbe JU, Lochhead RY, Thames SF. Polym Eng Sci 2007;47:374–80.
[30] Otaigbe JU, Jane J. J Environ Polym Degrad 1997;5:75–80.
[31] Wang W, Guo Y, Otaigbe JU. Polymer 2008;49:4393–8.
[32] Wu Q, Zhang L. Ind Eng Chem Res 2001;40:1879–83.
[33] Berkowitz SA, Velicelebi G, Sutherland JWH, Sturtevant JM. Proc Natl Acad Sci 1980;77:4425.